Facile Coating of Manganese Oxide on Tin Oxide Nanowires with High-Performance Capacitive Behavior

Jian Yan,[‡] Eugene Khoo,[†] Afriyanti Sumboja,[†] and Pooi See Lee[†,‡,*]

[†]School of Materials Science and Engineering, Nanyang Technological University, 50 Nanyang Avenue Blk N4.1, Singapore 639798 and [‡]Temasek Laboratories, Nanyang Technological University, Singapore 637553

ABSTRACT In this paper, a very simple solution-based method is employed to coat amorphous MnO_2 onto crystalline SnO_2 nanowires grown on stainless steel substrate, which utilizes the better electronic conductivity of SnO_2 nanowires as the supporting backbone to deposit MnO_2 for supercapacitor electrodes. Cyclic voltammetry (CV) and galvanostatic charge/discharge methods have been carried out to study the capacitive properties of the SnO_2/MnO_2 composites. A specific capacitance (based on MnO_2) as high as 637 F g^{-1} is obtained at a scan rate of 2 mV s^{-1} (800 F g^{-1} at a current density of 1 A g^{-1}) in 1 M Na_2SO_4 aqueous solution. The energy density and power density measured at 50 A g^{-1} are 35.4 W h kg^{-1} and 25 kW kg^{-1}, respectively, demonstrating the good rate capability. In addition, the SnO_2/MnO_2 composite electrode shows excellent long-term cyclic stability (less than 1.2% decrease of the specific capacitance is observed after 2000 CV cycles). The temperature-dependent capacitive behavior is also discussed. Such high-performance capacitive behavior indicates that the SnO_2/MnO_2 composite is a very promising electrode material for fabricating supercapacitors.

KEYWORDS: MnO_2 · SnO_2 · nanocomposite · supercapacitor

In recent decades, supercapacitors have attracted significant attention due to their high power density, longer cycle life than batteries, and higher energy density than conventional dielectric capacitors.[1−5] Such outstanding advantages make them good candidates for hybrid electric vehicles, large industrial equipment, and other renewable energy storage applications.[6,7] Depending on the charge storage mechanism, supercapacitors are generally classified into electrical double-layer capacitors (EDLCs) and pseudo-capacitors (or redox supercapacitors).[5,7] EDLCs, using carbon-based active materials with high surface area, build up electrical charge at the electrode/electrolyte interface. EDLCs usually have high power density but suffer from low capacitance and low rate capability. The pseudo-capacitors utilize fast and reversible surface or near-surface reactions for charge storage. Compared with EDLC-based capacitors, pseudo-capacitors based on transition metal oxides, nitrides, and conducting polymers could provide higher specific capacitance of the active materials but suffer from disadvantages such as higher cost, poor rate capability, and low conductivity.[8−13] Therefore, there is currently an impending need to improve their performance to meet the increasing urgent demand for energy storage and stringent requirements in a variety of potential applications.

Understanding the charge storage mechanism in pseudo-capacitive materials gives us clues and directive strategies in the realization of high-performance supercapacitors. To achieve high power and energy densities, high specific surface area, high electronic conductivity, and a fast cation intercalation/de-intercalation process are very important. Among the transition metal oxides, ruthenium oxides and hydroxides have shown the best performance.[8] However, their expensive nature limits their actual use on a large scale, which led to the study of low-cost metal oxides as alternatives, such as MnO_2, MoO_3, VO_x, and WO_3.[14−17] Recent reports show that supercapacitors based on thin films (thickness about several tens of nanometers) exhibit high specific capacitance due to their high specific surface area. For instance, a MnO_2 thin film provides capacitance as high as 698 F g^{-1}.[9] However, the area-normalized capacitance is unacceptable due to the low active mass. In general, transition metal oxides suffer from poor conductivity. Many groups have tried using carbon- or nitride-based metal oxide composites to improve the poor electronic conductivity. For example, Lu *et al.* synthesized V_2O_5/carbon nanotube hierarchical nanowire composites with a capacitance of 440 F g^{-1} at a current density of 0.25 A g^{-1}.[5] Liu *et al.* reported that the capacitance can reach 432 F g^{-1} for a 10 wt % loading

*Address correspondence to pslee@ntu.edu.sg.

Received for review March 23, 2010 and accepted June 24, 2010.

Published online July 1, 2010.
10.1021/nn100592d

© 2010 American Chemical Society

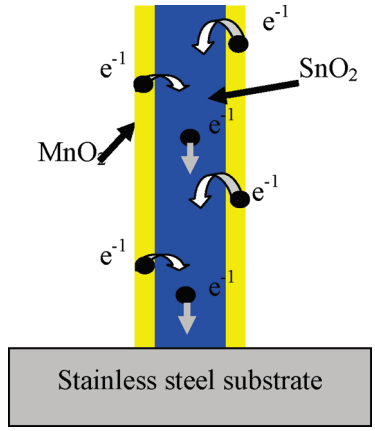

Scheme 1. Schematic image of the amorphous MnO_2 loaded on the SnO_2 nanowires grown on the stainless steel substrate. The SnO_2 nanowire provides a direct path for the electrons.

$Ni(OH)_2$/carbon nanotube composite at 10 mV s^{-1} scan rate.[2] Very recently, Fan *et al.* synthesized a carbon nanotube/MnO_2 composite using a microwave-assisted method, and capacitance as high as 944 F g^{-1} (85% of the theoretical value) was achieved at 1 mV s^{-1} scan rate for the low-loaded sample (carbon nanotube−15% MnO_2).[18] Such investigations intend to balance the cost and the performance of supercapacitors. However, the use of carbon nanotubes reduces the cost-effectiveness and deters potential deployment. Despite intensive research efforts, making supercapacitors with high energy density and power density still remains a challenge.

Due to its low cost and excellent capacitive performance in aqueous electrolyte, environmentally friendly MnO_2 has been considered a very promising material for supercapacitors.[9] In previous studies, SnO_2 nanowires synthesized by chemical vapor deposition had conductivity ranging from about 5 to 74 S cm^{-1}.[19−21] The conductivity of MnO_2 nanowires fabricated using a hydrothermal technique is about 8.6×10^{-4} S cm^{-1}.[22] MnO_2 nanorods synthesized by a solution-based method have a conductivity of 4.2×10^{-2} S cm^{-1}, and the conductivity of bulk MnO_2 semiconductors is about 8×10^{-2} S cm^{-1}.[23,24] This clearly shows that the conductivity of SnO_2 nanowires is about 2 orders of magnitude larger than that of MnO_2. Therefore, in this study we employ a facile method to coat amorphous MnO_2 on SnO_2 nanowires which have been grown onto a stainless steel (SS) substrate, as illustrated in Scheme 1, showing a SnO_2/MnO_2 core/shell nanostructure. This strategy has several advantages: (1) a thin layer of MnO_2 would enable a fast, reversible faradic reaction and provide a short ion diffusion path; (2) SnO_2 nanowires, with high conductivity, would provide a direct path for the electrons transport; and (3) SnO_2 nanowires would create channels for the effective transport of electrolyte. The SnO_2/MnO_2 composite shows a good capacitive performance. The specific capacitance reaches 637 F g^{-1} at a scan rate of 2 mV s^{-1}, and even higher, at 800 F g^{-1}, when tested by a constant current charge/discharge method. The temperature-dependent capacitive behavior is discussed. Excellent long-term cycle stability at room temperature and low temperature (3 °C) is obtained. These results suggest that the SnO_2/MnO_2 composite is a very promising electrode material for fabricating supercapacitors.

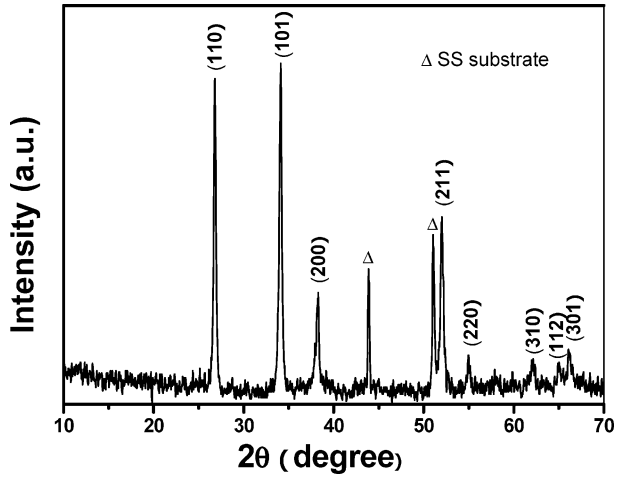

Figure 1. Typical XRD patterns of the as-synthesized SnO_2/MnO_2 sample The peaks marked with "Δ" belong to SS substrate.

RESULTS AND DISCUSSION

Microstructure Characterizations. Figure 1 shows typical X-ray diffraction (XRD) patterns of the as-prepared composite products. All the XRD peaks can be indexed to the tetragonal SnO_2 (JCPDS Card 88-0287), except the two peaks marked with "Δ" belonging to the stainless steel substrate. There is no peak pertaining to manganese oxide. This indicates that the manganese oxide is amorphous in nature.

Scanning electron microscopy (SEM) images of as-synthesized products are shown in Figure 2a,b. It can be seen that the nanowires are several micrometers long. The FE-SEM image with high magnification shows that the diameter of the nanowires is around 50 nm. Elemental analysis by energy-dispersive X-ray (EDX) spectroscopy reveals that the molar ratio of Sn and Mn is close to 1:0.33 (Figure S1, Supporting Information). Together with the mass measurement (tin oxide nanowires, 472 μg; manganese oxide, 80 μg), the composition of the manganese oxide can be identified as MnO_2. The low-magnification transmission electron microscopy (TEM) image in Figure 2c clearly shows that the SnO_2 nanowires with diameters about 40 nm were coated with a thin and brighter contrast layer, suggesting a core/shell structure. The shell is determined to be MnO_2, which will be discussed in the following. The thickness of the MnO_2 shell is several nanometers. The inset of Figure 2c is the corresponding selected area electron diffraction (SAED) pattern. There is only one set of diffraction patterns, which belongs to the tetragonal SnO_2. This result is further confirmed by HRTEM

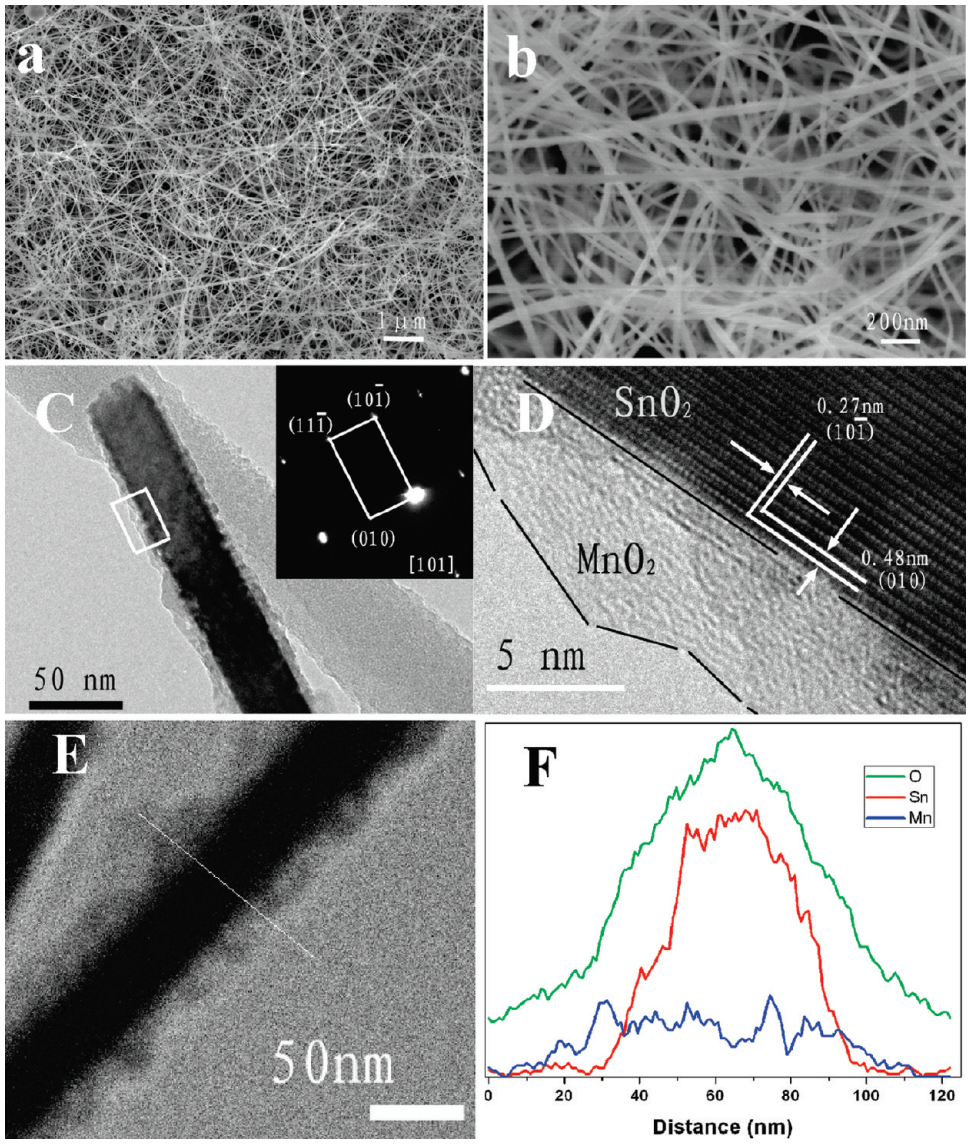

Figure 2. (a,b) Low- and high-maganification FE-SEM images of the SnO_2/MnO_2 composites showing that the length of the nanowires is several micrometers and their diameter is about 50 nm. (c) Low-magnification TEM image of the as-synthesized products, depicting that the SnO_2 nanowires are covered with a thin layer of MnO_2. The inset shows the SAED pattern. (d) Typical high-magnification TEM image of a single SnO_2/MnO_2 composite nanowire recorded from the area marked with a white rectangle in panel c. (e,f) TEM image and line-scanning (indicated by a line in panel e) elemental mapping showing O, Sn, and Mn elemental profiles across the SnO_2/MnO_2 core/shell nanowires.

examination. As shown in Figure 2d, recorded from the area marked by the white rectangle in Figure 2c, the marked interplanar *d* spacings (of 0.48 and 0.27 nm) correspond to the (010) and (10$\bar{1}$) lattice planes of the tetragonal SnO_2, respectively. The amorphous MnO_2 shell is indicated by black lines in Figure 2d. This result agrees well with the XRD characterization. The spatial distributions of the atomic contents across the SnO_2/MnO_2 nanowire are obtained by EDS line-scanning (indicated by a line in Figure 2e) elemental mappings of O, Sn, and Mn (see Figure 2f). The profile of Sn shows a peak which is located at the center of the Mn profile. This result directly shows the core/shell configuration.[25,26] Analysis of the data shows that the diameter of the SnO_2 core and the total outer diameter of the composite nanowire are about 40 and 80 nm, respectively, consistent with the TEM image (Figure 2e). This core/shell configuration is expected to achieve high performance: the thin MnO_2 shell is beneficial to the fast faradic reaction, which would enable high specific capacitance, and the SnO_2 core nanowire serves as a fast path for electron transport, which would enable high power density. This will be discussed in detail in the following.

In this work, the amorphous MnO_2 layer was obtained by the reduction of Mn(VII) species from $KMnO_4$ solution according to the following reaction:

$$MnO_4^- + 4H^+ + 3e^- \rightarrow MnO_2 + 2H_2O \qquad (1)$$

As there is no reducing agent introduced during the coating process, the electrons are expected to be

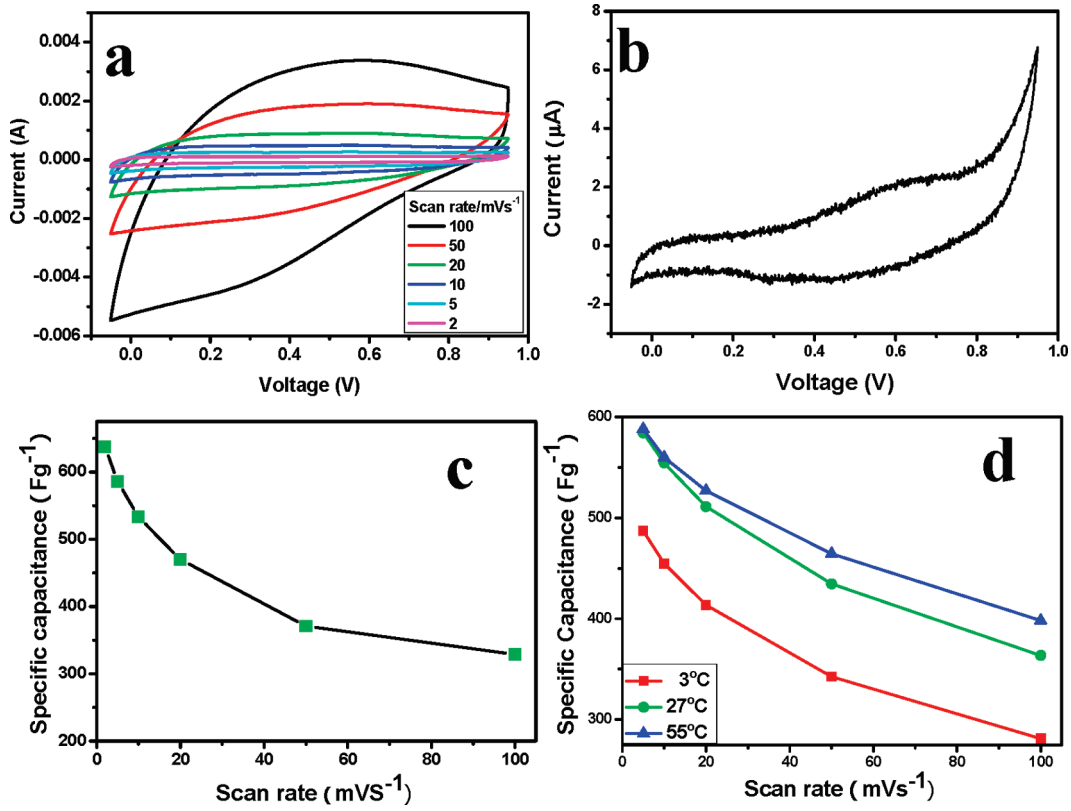

Figure 3. (a) Cyclic voltammetry (CV) curves of the SnO_2/MnO_2 composites at different scan rates in 1 M Na_2SO_4 aqueous solution. (b) CV curve of SnO_2 nanowires (705 μg) grown on the SS substrate at a scan rate of 2 mV s^{-1}. (c) Plotted curve of the variation in the specific capacitance of the SnO_2/MnO_2 composites as a function of the scan rate. (d) Specific capacitance obtained at different scan rates at 3, 27, and 55 °C.

supplied by the stainless steel substrate. This statement is based on the following experiment results: (1) When the stainless steel substrate was immersed into $KMnO_4$ solution, a black layer of MnO_2 was formed on its surface. (2) If the substrate was replaced with Si, it was difficult to coat MnO_2 on the SnO_2 nanowires grown on the Si substrate. Even when the temperature was kept at 95 °C for more than 24 h, the loading amount of MnO_2 was around 5 wt % or less and the thickness of the MnO_2 shell was not uniform. (3) If the substrate was replaced with Ni foam, MnO_2 could be coated on the SnO_2 nanowires with similar loading amount using the same condition. These results suggest that metallic substrate might be responsible for the facile coating process. One possible reason is that the metallic substrate contains free electrons which might transport to the SnO_2 nanowires for the reduction of Mn(VII) during the coating process.

During the coating process, the growth temperature determines the growth rate of the MnO_2 shell. The growth rate could be accelerated at higher temperature (90−95 °C) or decelerated at lower temperature (80 °C or lower). For better control of the coating process, moderate temperature (85 °C) was selected for the growth of the MnO_2 shell. The annealed sample shows better stability (see the following cycling stability measurement). However, when the sample was annealed at higher temperature (470 °C for 1 h), the MnO_2 shell transformed to cubic Mn_2O_3 (JCPDS Card 894836; XRD pattern is shown in Figure S2 in the Supporting Information).

Electrochemical Analysis. Figure 3a shows the cyclic voltammetry (CV) curves of the SnO_2/MnO_2 composites at different scan rates in 1 M Na_2SO_4 aqueous solution. The specific capacitance of the electrode was calculated from the CVs according to the following equation,

$$C = \frac{Q}{\Delta V\, m} \qquad (2)$$

where C (F g^{-1}) is the specific capacitance, m (g) is the mass of the MnO_2 in the electrodes, Q (C) is the average charge during the charging and discharging process, and ΔV (V) is the potential window. It is noteworthy that the capacitance contribution from SnO_2 nanowires is negligible due to the following two attributes. First, the SnO_2 nanowires were coated with a MnO_2 shell and could rarely take part in the charge-storing process, in which the charge is stored at the surface or near the surface of the electrode materials through the faradic reaction. The second direct evidence is the measured specific capacitance of SnO_2 nanowires grown on the stainless steel substrate, which is as low as 0.5 F g^{-1} at 2 mV s^{-1} scan rate, as shown by the CV curve of SnO_2 nanowires in Figure 3b. The variation in the specific

capacitance of the SnO_2/MnO_2 composites as a function of the scan rate is plotted in Figure 3c. The CV curves at high scan rates are not perfectly rectangular. This is improved at low scan rates as shown in Figures 3a, S3, and S4, suggesting that polarization is one of the reasons.[14,27,28] At a high scan rate, the ions on the electrode decrease rapidly with increasing current, while the ions in the electrolyte diffuse too slowly to (and, because of the ions on the interface, *cannot*) satisfy the need of ions near the interface during the charge and discharge process.[28,29] This leads to the non-ideal rectangular shape of the CV curves. A more detailed investigation is underway to understand the origin of this characteristic. The value of specific capacitance reaches as high as 637 F g^{-1} at 2 mV s^{-1} scan rate. At a high scan rate of 100 mV s^{-1}, the specific capacitance still remains at 329 F g^{-1}. In a previous study, it was reported that the specific capacitance of a 45 μg cm^{-2} manganese oxide film prepared by cathodic electrodeposition on stainless steel substrate was 353 F g^{-1} at a scan rate of 2 mV s^{-1}. However, at a high scan rate of 100 mV s^{-1}, the specific capacitance was only 135 F g^{-1}.[30] In our case, the MnO_2 loaded on SnO_2 nanowires retains a high specific capacitance at a high scan rate. Such high specific capacitance and good rate capability are attributed to the unique core/shell nanostructure. As reported in previous studies, the charge storage mechanism of amorphous MnO_2 is mainly a surface process, which involves the intercalation/de-intercalation of alkali cations.[14,31]

$$(MnO_2)_{surface} + M^+ + e^- \leftrightarrow (MnOOM)_{surface} \quad (M = Li^+, Na^+, K^+, \text{or } H_3O^+) \tag{3}$$

A thin MnO_2 layer loaded on SnO_2 nanowires with small diameters has high surface area, which provides more sites for the adsorption of Na^+. This endows a high specific capacitance. As indicated by the above equation, cations and electrons both take part in the charge/discharge process. Obviously, the diffusion of the cations in the MnO_2 layer and the transport of electrons would affect the rate of the charge/discharge process. In our case, the thin MnO_2 layer, with a short diffusion path, can indeed provide an ideal pathway for ion transport.[32] In addition, the core SnO_2 nanowire, with much higher conductivity than that of MnO_2, serves as a fast path for the transport of electrons. These unique characteristics give competitive advantages to the SnO_2/MnO_2 core/shell nanostructure-based supercapacitor. These analyses are in accord with the above experimental results. SnO_2/MnO_2 composites with different MnO_2 loading amounts were obtained by controlling the immersion time. The CV curves and specific capacitance (Figure S3−S5, Supporting Information) indicate that the lower-loading sample has a higher electrochemical utilization of MnO_2 in the SnO_2/MnO_2 composites, in agreement with a previous report.[18]

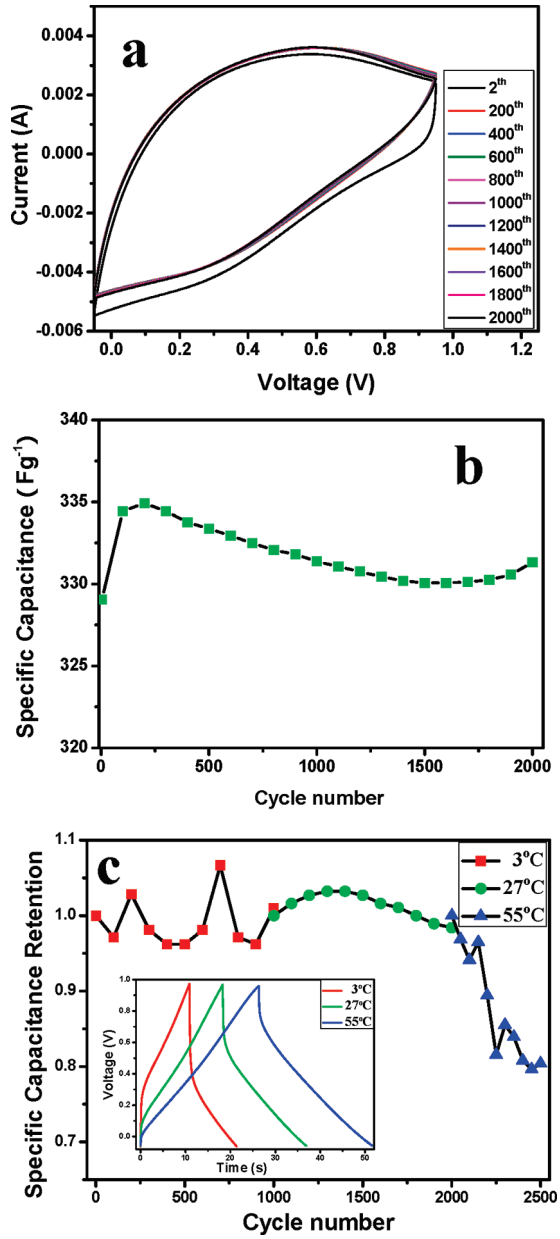

Figure 4. (a) Cyclic voltammetry curves of the 2nd to 2000th cycles of the SnO_2/MnO_2 composites, measured in 1 M Na_2SO_4 aqueous solution at a scan rate of 100 mV s^{-1}. (b) Plotted curve of the variation in the specific capacitance of the SnO_2/MnO_2 composites as a function of the cycle number. (c) Curve showing long-term stability as a function of the cycle number tested by constant current charge/discharge method (current density of 20 A g^{-1}), which was carried out continuously at 3 ± 1 °C (ice water bath), then 27 °C (room-temperature), and finally 55 ± 2 °C (water bath). The inset shows the first cycle of charge/discharge curves at different temperatures at a high current density of 20 A g^{-1}.

Temperature has an important influence on supercapacitor cells. It is valuable to evaluate the capacitive behavior of SnO_2/MnO_2 composites at various temperatures. Figure 3d shows the specific capacitance obtained at different temperatures and scan rates. It clearly shows that the specific capacitance and rate

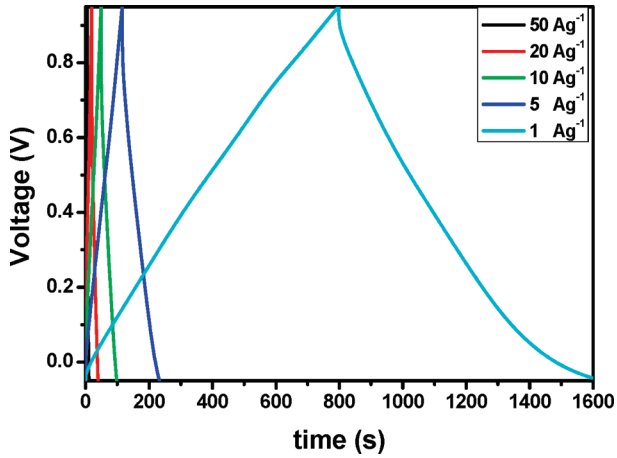

Figure 5. Constant current charge/discharge curves of the as-prepared SnO_2/MnO_2 composites at different current density.

capability increase with increasing temperature. This is attributed to the decrease of effective internal resistance with increasing temperature, as reported previously.[33−37] Note that at low temperature (3 °C), the specific capacitance still remains 83% compared to the one obtained at room temperature (27 °C). The specific capacitance does not increase much at high temperature (55 °C) at a low scan rate (5 mV s^{-1}), which might be due to nonuniform thickness of the MnO_2 shell. Some of the thick MnO_2 shell might not take part into the charge storage process. However, at a high scan rate (100 mV s^{-1}), the specific capacitance increases noticeably, indicating that the rate capability at high temperature (55 °C) is further improved.

The long-term cycle stability of the as-synthesized composites was evaluated by repeating the CV test at a scan rate of 100 mV s^{-1} for 2000 cycles. The CV curves and the specific capacitance as a function of cycle number are presented in Figure 4. It can be seen that all the CV curves (except the second cycle) are almost overlapping with each other, indicating a good cycling stability. The specific capacitance increases slightly at the beginning (from the initial 329 F g^{-1} to a maximum of 335 F g^{-1} at the 200th cycle) and subsequently decreases slightly (from the maximum of 335 F g^{-1} to 330 F g^{-1} at the 1600th cycle). It is interesting that specific capacitance increases a little after the 1600th cycle. After 2000 cycles, the decrease of specific capacitance is less than 1.2% of the maximum specific capacitance. The electrolyte remains transparent, indicating minimal dissolution of MnO_2 into the solution after the cycling test, which is the main cause of capacitance loss of MnO_2-based capacitors.[9,38] These results demonstrate that the as-prepared sample, as an active electrode material, is very stable during the cycling test. After the cycling test, no obvious morphology change can be observed through SEM and TEM characterization (Figure S6, Supporting Information).

Constant current charge/discharge method, which is important for the evaluation of supercapacitor, has also been employed to test the long-term stability at various temperatures. The measurement was continuously carried out at 3 ± 1 °C (ice water bath), then 27 °C (room-temperature), and finally 55 ± 2 °C (water bath). The results are shown in Figure 4c. The inset shows the first cycle of charge/discharge curves at different temperatures at a high current density of 20 A g^{-1}. Clearly, the *iR* drop decreases with increasing temperature indicating the decrease of effective internal resistance, which is consistent with the above analysis. The specific capacitances obtained at 3, 27, and 55 °C are 210, 372, and 510 F g^{-1}, respectively. Although the specific capacitance fluctuated during the long-term cycling test at low and high temperature due to the temperature variation, the result still shows that there is no obvious attenuation of capacitance at low temperature. At room temperature, the attenuation of capacitance is only 1.6% after 1000 cycles, indicating excellent stability, which agrees with the CV measurements. But at high temperature the stability is not as good as that at lower temperature. The attenuation of capacitance is about 20% after 500 cycles. The electrolyte becomes a little light yellow after the cycling test at 55 °C, indicating that the dissolution is responsible for the capacitance loss. These results suggest that the as-synthesized SnO_2/MnO_2 composites are suitable for operation at lower temperature, which is important for many applications of supercapacitors, as reported previously.[34]

Current density is one of the important factors influencing the capacitive behavior of the supercapacitor. The constant current charge/discharge curves of the as-prepared SnO_2/MnO_2 composites at different current densities are shown in Figure 5. The charging curves are very symmetric with their corresponding discharge counterparts. Notably, the voltage loss is low even at a high current density of 5 A g^{-1}, indicating that the internal resistance is low. The discharge specific capacitance is calculated from the discharge curves using the following formula:

$$C = \frac{I\,\Delta t}{m\,\Delta V} \tag{4}$$

where I (A), Δt (s), m (g), and ΔV (V) are the discharge current, discharge time consumed in the potential range of ΔV, mass of the active materials (or mass of the total electrode materials), and the potential windows, respectively. The results are listed in Table 1. As can be seen, the specific capacitance obtained at the current density of 1 A g^{-1} is as high as 800 F g^{-1}. It is

TABLE 1. Specific capacitance, power density, and energy density of the SnO_2/MnO_2 composites at different current densities (based on the mass of MnO_2)

curr ent density (A g^{-1}) =	50	20	10	5	1
specific capacitance (F g^{-1}) =	255	400	496	586	800
power density (kW kg^{-1})	25	10	5	2.5	0.5
energy density (W h kg^{-1})	35.4	55.5	68.8	81.4	111

higher than that obtained by the CV test. This is in agreement with a previous work, which reported that the specific capacitance obtained by the constant current charge method is higher than that obtained by the CV method.[9] This might be because, at low current density, it allows more time for the cations to intercalate into the MnO_2. At a very high current density of 50 A g^{-1}, the specific capacitance reaches 255 F g^{-1}, demonstrating the good rate capability once again.

Power density and energy density are important parameters for the investigation of the electrochemical performance of the electrochemical cells. They have been used to evaluate the performance of the as-prepared composite electrode. The power density and energy density calculated from the following equations are shown in Table 1:

$$E = \frac{1}{2}C(\Delta V)^2 \quad (5)$$

$$P = \frac{E}{t} \quad (6)$$

where P (kW kg^{-1}), C (F g^{-1}), ΔV (V), t (s), and E (W h kg^{-1}) are the power density, specific capacitance, potential window of discharge, discharge time, and energy density, respectively. It can be seen that the energy density and power density, calculated on the basis of the mass of the active materials (MnO_2), reach 35.4 W h kg^{-1} and 25 kW kg^{-1}, respectively. Importantly, the power density could reach the power target of the Partnership for a New Generation of Vehicles (PNGV), 15 kW kg^{-1}.[3,18] At lower power density, the energy density reaches as high as 111 W h kg^{-1}. Such energy and power performance is highly competitive with that of Ni-MH batteries and significantly better than that of current electrochemical capacitors, based on data from recent literature.[5,7] These results suggest that the SnO_2/MnO_2 composite is a very promising electrode material for fabricating supercapacitors.

CONCLUSIONS

In this paper, a simple, quick immersion approach to coat amorphous MnO_2 on SnO_2 nanowires was developed. The specific capacitance based on the MnO_2 is 637 and 329 F g^{-1} at scan rates of 2 and 100 mV s^{-1}, respectively. The specific capacitance obtained by the constant current charge/discharge method is even higher (800 F g^{-1} obtained at a current density of 1 A g^{-1}). The energy density and power density, measured at 50 A g^{-1}, are 35.4 W h kg^{-1} and 25 kW kg^{-1}, respectively, demonstrating the good rate capability. The temperature-dependent capacitive behavior is discussed. Excellent long-term cycle stability at room temperature and low temperature (3 °C) is obtained. Such good performance is primarily attributed to the core/shell structure. The thin amorphous MnO_2 shell is beneficial for the fast faradic reaction, which enables high specific capacitance, and the SnO_2 core nanowire serves as a fast path for electron transport and increases the electrochemical utilization of amorphous MnO_2. The work highlights the realization of high electrochemical activity of MnO_2 coated on SnO_2 nanowires, which serve as a good current collector. The as-prepared amorphous MnO_2 loaded on the SnO_2 nanowires is very suitable and promising for fabricating supercapacitors.

METHODS

Synthesis of SnO_2 Nanowires. The synthesis of SnO_2 nanowires was carried out in a high-temperature horizontal quartz tube furnace system. Mixed SnO_2 powder and carbon powders (molar ratio 1:1) were loaded at the center of the furnace. Before heating, the system was pumped to 1.3×10^{-2} mbar. The central temperature was then increased to 910 °C at a rate of 15 °C min^{-1} and kept for 40 min under a constant Ar flow of 40 sccm. Stainless steel substrate (SS substrate; other substrate, such as, Si or Ni foam might be also used) coated with 3 nm thick Au film was placed at the lower temperature region (around 600 °C) to collect the products. It should be noted that the source materials and SS substrate were placed in a small tube (inner diameter about 1.7 cm) with one end open. The pressure inside the tube was around 0.5 mbar during the growth process. Subsequently, the furnace was cooled to room temperature. The mass of the SnO_2 nanowires (472 μg) is the weight difference of the sample before and after the growth process, measured using a microbalance with an accuracy of 1 μg. The area of the substrate is about 1 cm^2.

Coating MnO_2 on SnO_2 Nanowires. The precursor solution for the coating process was prepared by mixing 5 mmol of $KMnO_4$ (reagent grade) and 5 mmol of H_2SO_4 into 50 mL of deionized water. The SS substrate grown with SnO_2 nanowires was immersed into the solution, which was kept at 85 °C using a hotplate. The duration of immersion was 60 min. The loading amount of MnO_2 can be easily controlled by adjusting the immersion time. Next, the sample was rinsed with deionized water and subsequently annealed at 400 °C for 5 min using a hotplate in air. The loading amount of the MnO_2 (80 μg) is the weight difference of the sample before and after the coating process, measured using a microbalance. The as-synthesized sample was flushed with water or dropped from a height of 2 m onto the floor; no damage was observed, indicating a relatively good adhesion of the SnO_2/MnO_2 core/shell nanowires and the substrate. However, the nanowire-based film could be scraped from the substrate by a blade or other sharp tool.

Characterization. The phase of the product was identified by X-ray powder diffraction (Shimadzu) using Cu Kα ($\lambda = 0.15406$ nm) radiation at 50 kV and 50 mA in a 2θ range from 10° to 70° at room temperature. The morphology and structure of the products were characterized by field emission scanning electron microscopy (JEOL 6340F), transmission electron microscopy (JEOL 2010&2100F), and high-resolution transmission electron microscopy with an X-ray energy-dispersive spectrometer. The chemical compositions were analyzed using energy-dispersive spectroscopy attached to the SEM (JEOL 6360) system.

Electrochemical Measurement. Electrochemical measurements were carried out using an electrochemical analyzer (Autolab Potentiostat, PGSTAT302N). The three-electrode cell consisted of Ag/AgCl as the reference electrode, Pt as the counter electrode, and the as-synthesized sample as the working electrode. A 1 M Na_2SO_4 solution served as electrolyte at room temperature. Cyclic voltammetry was done at different scan rates of 2, 5, 10, 20, 50, and 100 mV s^{-1}. The temperature-dependent specific capacitance was measured at 3 ± 1 (ice−water bath), 27 (room temperature), and 55 ± 2 °C (water bath) using CV. The constant

current charge/discharge method was employed to test the long-term stability at various temperatures. The measurement was continuously carried out at 3 ± 1 (ice−water bath), 27 (room temperature), and finally 55 ± 2 °C (water bath). Note that another sample (SnO_2/MnO_2, 374/55 μg) was used to test the temperature-dependent long-term stability. Galvanostatic charge/discharge curves were measured at different current densities of 1, 5, 10, 20, and 50 A g^{-1} to evaluate the power density and energy density. A potential window in the range from −0.05 to 0.95 V was used in all the measurements.

Supporting Information Available: EDS spectra of the SnO_2/MnO_2 composites; XED pattern of the sample annealed at 470 °C for 1 h; CV curves of the low and high loading samples; plotted curves of the variation in the specific capacitance of the SnO_2/MnO_2 composites as a function of the scan rate; and SEM and high-magnification TEM images of SnO_2/MnO_2 core/shell nanowire after cycling stability measurement. This material is available free of charge *via* the Internet at http://pubs.acs.org.

REFERENCES AND NOTES

1. Lee, M. T.; Tsai, W. T.; Deng, M. J.; Cheng, H. F.; Sun, I. W.; Chang, J. K. Pseudocapacitance of MnO_2 Originates From Reversible Insertion/Desertion of Thiocyanate Anions Studied Using in situ X-ray Absorption Spectroscopy in Ionic Liquid Electrolyte. *J. Power Sources* **2010**, *195*, 919–922.
2. Liu, C. G.; Lee, Y. S.; Kim, Y. J.; Song, I. C.; Kim, J. H. Electrochemical Characteristics of Hydrothermally Deposited Nickel Hydroxide on Multi-walled Carbon Nanotube for Supercapacitor Electrode. *Synth. Met.* **2009**, *159*, 2009–2012.
3. Wang, D. W.; Li, F.; Liu, M.; Lu, G. Q.; Cheng, H. M. 3D Aperiodic Hierarchical Porous Graphitic Carbon Material for High-Rate Electrochemical Capacitive Energy Storage. *Angew. Chem., Int. Ed.* **2008**, *47*, 373–376.
4. Chuen-Chang Lin, C. C.; Hung-Wei Chen, H. W. Coating Manganese Oxide onto Graphite Electrodes by Immersion for Electrochemical Supercapacitors. *Electrochim. Acta* **2009**, *54*, 3073–3077.
5. Chen, Z.; Qin, Y. C.; Weng, D.; Xiao, Q. F.; Peng, Y. T.; Wang, X. L.; Li, H. X.; Wei, F.; Lu, Y. F. Design and Synthesis of Hierarchical Nanowire Composites for Electrochemical Energy Storage. *Adv. Funct. Mater.* **2009**, *19*, 3420–3426.
6. Choi, D. W.; Blomgren, G. E.; Kumta, P. N. Fast and Reversible Surface Redox Reaction in Nanocrystalline Vanadium Nitride Supercapacitors. *Adv. Mater.* **2006**, *18*, 1178–1182.
7. Simon, P.; Gogotsi, Y. Materials for Electrochemical Supercapacitor. *Nat. Mater.* **2008**, *7*, 845–854.
8. Hu, C. C.; Chang, K, H; Lin, M. C.; Wu, Y. T. Design and Tailoring of the Nanotubular Arrayed Architecture of Hydrous RuO_2 for Next Generation Supercapacitors. *Nano Lett.* **2006**, *6*, 2690–2695.
9. Pang, S. C.; Anderson, M. A.; Chapmanb, T. W. Novel Electrode Materials for Thin-Film Ultracapacitors: Comparison of Electrochemical Properties of Sol-Gel-Derived and Electrodeposited Manganese Dioxide. *J. Electrochem. Soc.* **2000**, *147*, 444–450.
10. Qua, Q. T.; Shi, Y.; Li, L. L.; Guo, W. L.; Wua, Y. P.; Zhang, H. P.; Guan, S. Y.; Holze, R. $V_2O_5 \cdot 0.6H_2O$ Nanoribbons as Cathode Material for Asymmetric Supercapacitor in K_2SO_4 Solution. *Electrochem. Commun.* **2009**, *11*, 1325–1328.
11. Chen, C. L.; Zhao, D. L.; Xua, D.; Wang, X. K. γ-Mo_2N/Co_3Mo_3N Composite Material for Electrochemical Supercapacitor Electrode. *Mater. Chem. Phys.* **2006**, *95*, 84–88.
12. Zhou, X. P.; Chen, H. Y.; Shu, D.; He, C.; Nan, J. M. Study on the Electrochemical Behavior of Vanadium Nitride as A Promising Supercapacitor Material. *J. Phys. Chem. Solids* **2009**, *70*, 495–500.
13. Wang, Y. G.; Li, H. Q.; Xia, Y. Y. Ordered Whiskerlike Polyaniline Grown on the Surface of Mesoporous Carbon and Its Electrochemical Capacitance Performance. *Adv. Mater.* **2006**, *18*, 2619–2623.
14. Toupin, M.; Brousse, T.; Be'langer, D. Charge Storage Mechanism of MnO_2 Electrode Used in Aqueous Electrochemical Capacitor. *Chem. Mater.* **2004**, *16*, 3184–3190.
15. Farsi, H.; Gobal, F.; Raissi, H.; Moghiminia, S. J. The pH Effects on the Capacitive Behavior of Nanostructured Molybdenum Oxide. *Solid State Electrochem.* **2010**, *14*, 681–686.
16. Zeng, H. M.; Zhao, Y.; Hao, Y. J.; Lai, Q. Y.; Huang, J. H.; Ji, X. Y. Preparation and Capacitive Properties of Sheet V_6O_{13} for Electrochemical Supercapacitor. *J. Alloys Compd.* **2009**, *477*, 800–804.
17. Huang, C. C.; Xing, W.; Zhuo, S. P. Capacitive Performances of Amorphous Tungsten Oxide Prepared by Microwave Irradiation. *Scr. Mater.* **2009**, *61*, 985–987.
18. Yan, J.; Fan, Z. J.; Wei, T.; Cheng, J.; Shao, B.; Wang, K.; Song, L. P.; Zhang, M. L. Carbon Nanotube/MnO_2 Composites Synthesized by Microwave-Assisted Method for Supercapacitors with High Power and Energy Densities. *J. Power Sources* **2009**, *194*, 1202–1207.
19. Arnold, M. S.; Avouris, P.; Pan, W. Z.; Wang, Z. L. Field-Effect Transistors Based on Single Semiconducting Oxide Nanobelts. *J. Phys. Chem. B* **2003**, *107*, 659–663.
20. Ma, Y. J.; Zhou, F.; Lu, L.; Zhang, Z. Low-Temperature Transport Properties of Individual SnO_2 Nanowires. *Solid State Commun.* **2004**, *130*, 313–316.
21. Zhang, Y.; Kolmakov, A.; Lilach, Y.; Moskovits, M. Electronic Control of Chemistry and Catalysis at the Surface of an Individual Tin Oxide Nanowire. *J. Phys. Chem. B* **2005**, *109*, 1923–1929.
22. Cheng, F. Y.; Su, Y.; Liang, T.; Tao, Z. L.; Chen, T. MnO_2-Based Nanostructures as Catalysts for Electrochemical Oxygen Reduction in Alkaline Media. *Chem. Mater.* **2010**, *22*, 898–905.
23. Yang, Y.; Chong Xie, C.; Ruffo, R.; Peng, H. L.; Kim, D. K.; Cui, Y. Single Nanorod Devices for Battery Diagnostics: A Case Study on $LiMn_2O_4$. *Nano Lett.* **2009**, *9*, 4109–4114.
24. Kanda, M.; Yamda, S.; Shirogami, T.; Sato, Y.; Takamura, T. Solid-State Li/MnO_2 Cells. *J. Appl. Electrochem.* **1982**, *12*, 599–606.
25. Hu, J. Q.; Bando, Y.; Liu, Z. W.; Sekiguchi, T.; Golberg, D.; Zhan, J. H. Epitaxial Heterostructures: Side-to-Side Si-ZnS, Si-ZnSe Biaxial Nanowires, and Sandwichlike ZnS-Si-ZnS Triaxial Nanowires. *J. Am. Chem. Soc.* **2003**, *125*, 11306–11313.
26. Lauhon, L. J.; Gudiksen, M. S.; Deli Wang, D. L.; Charles M. Lieber, C. M. Epitaxial core-shell and core-multishell nanowire heterostructures. *Nature* **2002**, *420*, 57–61.
27. Adelkhaniz, H. Functionalized Electrolytic Manganese Dioxide Nanostructure Prepared at Fixed pH for Electrochemical Supercapacitor. *J. Electrochem. Soc.* **2009**, *156*, A791–A795.
28. Wang, H.; Tang, Z. Y.; Sun, L.; He, Y. B.; Wu, Y. X.; Li, Z. Y. Capacitance Performance Enhancement of TiO_2 Doped with Ni and Graphite. *Rare Metals* **2009**, *28*, 231–236.
29. Jayalakshmi, M.; Rao, M. M.; Venugopal, N.; Kim, K. B. Hydrothermal Synthesis of SnO_2-V_2O_5 Mixed Oxide and Electrochemical Screening of Carbon Nano-tubes(CNT), V_2O_5, V_2O_5-CNT, and SnO_2- V_2O_5-CNT Electrodes for Supercapacitor Applications. *J. Power Sources* **2007**, *166*, 578–583.
30. Wei, J.; Nagarajan, N.; Zhitomirsky, I. Manganese Oxide Films for Electrochemical Supercapacitors. *J. Mater. Proc. Technol.* **2007**, *186*, 356–361.
31. Ni, J. P.; Lu, W. C.; Zhang, L. M.; Yue, B. H.; Shang, X. F.; Lv, Y. Low-Temperature Synthesis of Monodisperse 3D Manganese Oxide Nanoflowers and Their Pseudocapacitance Properties. *J. Phys. Chem. C* **2009**, *113*, 54–60.
32. Zhang, L. L.; Li, S.; Zhang, J. T.; Guo, P. Z.; Zheng, J. T.; Zhao, X. S. Enhancement of Electrochemical Performance of Macroporous Carbon by Surface Coating of Polyaniline. *Chem. Mater.* **2010**, *22*, 1195–1202.

33. Masarapu, C.; Zeng, H. F.; Huang, K. H.; Wei, B. Q. Effect of Temperature on the Capacitance of Carbon Nanotube Supercapacitors. *ACS Nano* **2009**, *3*, 2199–2206.
34. Liu, X. R.; Peter G. Pickup, P. G. Performance and Low Temperature Behaviour of Hydrous Ruthenium Oxide Supercapacitors with Improved Power Densities. *Energy Environ. Sci.* **2008**, *1*, 494–500.
35. Yuan, C. Z.; Zhang, X. G.; Wu, Q. F.; Gao, B. Effect of Temperature on the Hybrid Supercapacitor Based on NiO and Activated Carbon with Alkaline Polymer Gel Electrolyte. *Solid State Ionics* **2006**, *177*, 1237–1242.
36. Liu, P.; Verbrugge, M.; Soukiazian, S. Influence of Temperature and Electrolyte on the Performance of Activated-Carbon Supercapacitors. *J. Power Sources* **2006**, *156*, 712–718.
37. Kotz, P.; Hahna, M.; Gallay, R. Temperature Behavior and Impedance Fundamentals of Supercapacitors. *J. Power Sources* **2006**, *154*, 550–555.
38. Era, A.; Takehara, Z.; Yoshizawa, S. Discharge Mechanism of The Manganses Oxide Electrode. *Electrochim. Acta* **1967**, *12*, 1199–1212.